Chemical Science

ROYAL SOCIETY OF CHEMISTRY

EDGE ARTICLE

View Article Online
View Journal

Check for updates

Cite this: DOI: 10.1039/d6sc02577c

All publication charges for this article have been paid for by the Royal Society of Chemistry

Imidazoliumyl-substituted di- and iso-tetraphosphanes and their metal-mediated fragmentation reactions

Jannis Fidelius, †[a] Clemens Taube,†[a] Kai Schwedtmann, [a] Felix Hennersdorf, [a] Rosa M. Gomila, [c] Antonio Frontera, [c] Robert Wolf *[b] and Jan J. Weigand *[a]

Received 28th March 2026
Accepted 27th May 2026

DOI: 10.1039/d6sc02577c

rsc.li/chemical-science

Monocationic imidazoliumyl-substituted phosphanes, $L_CP(R)Cl^+$ (L_C = 1,3-diisopropyl-4,5-dimethylimidazol-2-yl), were synthesized as their respective triflate salts **2a–c**[OTf] (a: R = Cy; b: R = Ph; c: R = Py). These serve as versatile building blocks for the formation of the corresponding imidazoliumyl-substituted diphosphanes ($(L_CPR)_2$ **5a–c**$[OTf]_2$) and iso-tetraphosphanes ($(L_CPR)_3P[OTf]_3$ **6a,b**$[OTf]_3$). The introduction of a cationic (onio) substituent substantially alters the preferred reaction pathways of the P-scaffolds compared to their neutral congeners and electronically predisposes selected P–P bonds toward fragmentation. DFT calculations reveal a strong localization of the LUMO orbitals on the P–P bond, indicating susceptibility to nucleophilic attack. Both **5a,b**$[OTf]_2$ and **6a**$[OTf]_3$ undergo metal-mediated fragmentation reactions. Reactions of **5a,b**$[OTf]_2$ with $Pd(PPh_3)_4$ afford two distinct dinuclear complexes, while reactions of **6a**$[OTf]_3$ with metal chlorides yield triphosphanide complexes $(L_CPCy)_2PM[OTf]_2$ **9**$[OTf]_2$: M = Pd(allyl), **10**$[OTf]_2$: M = $Au(PPh_3)$, accompanied by the formation of **2a**[OTf]. Treatment of **6a**$[OTf]_3$ with the NHC IPr (1,3-diisopropyl-4,5-dimethylimidazol-2-ylidene) provides the free triphosphanide ligand $(L_CPCy)_2P[OTf]$ (**11**[OTf]).

Introduction

The importance of tertiary phosphanes (R_3P) as ligands in organometallic chemistry, both in fundamental research and in industry, cannot be overstated. In particular, the facile fine-tuning of steric and electronic properties of the P atom through alteration of the substituents has led to the development of neutral and, more recently, cationic (onio-)substituted phosphorus ligand systems.[1,2] Similarly, neutral diphosphanes of type R_4P_2 (R = alkyl, aryl) are potent ligands for mono- and bimetallic complexes,[3,4] comprising various coordination modes while typically preserving the central P–P bond (Fig. 1-I).[5] In contrast, despite several synthetic approaches, the coordination chemistry of related triphosphanes R_5P_3 remains far less explored and is mainly limited to transition metal carbonyls (Fig. 1-II).[6] The limited availability of iso-tetraphosphanes R_6P_4 (ref. 7–11) is mainly attributed to scrambling reactions[8,11] which hinder the syntheses of larger catenated and branched structures compared to their cyclic derivatives.

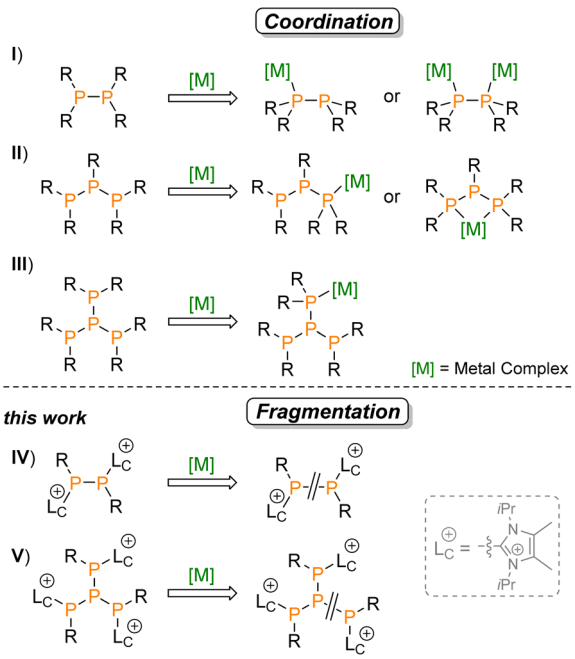

Fig. 1 Coordination behaviour of neutral branched and catenated oligophosphanes (top, I–III) and fragmentation reactions of cationic derivatives (bottom, IV and V); (L_C = 1,3-diisopropyl-4,5-dimethylimidazole-2-yl).

[a]Faculty of Chemistry and Food Chemistry, Technische Universität Dresden, 01062 Dresden, Germany. E-mail: jan.weigand@tu-dresden.de

[b]Institute of Inorganic Chemistry, Universität Regensburg, 93040 Regensburg, Germany

[c]Department of Chemistry, Universitat de Illes Balears, 07122 Palma de Mallorca, Spain

† These authors contributed equally to this work.

As a result, there is a notable lack of detailed studies on the reactivity of these systems towards transition metals. To the best of our knowledge, only one iron carbonyl complex has been structurally characterized (Fig. 1-III).[11]

Beyond neutral oligophosphanes, the coordination chemistry of phosphorus-centered cations has garnered considerable interest over the last decade.[12] Recently, we reported the synthesis of various cationic polyphosphanes that exhibit metal-dependent coordination and insertion reactions.[13,14] Key to the formation of stable cationic oligophosphanes is the introduction of imidazoliumyl substituents, which enables precise electronic tuning of the attached phosphorus atoms,[2,15] allowing for the stabilization of a wide range of phosphorus bonding motifs.[16,17] Our access to imidazoliumyl-substituted chlorophosphane salts of the type $L_CP(R)Cl[OTf]$[17] motivated us to explore their potential in constructing imidazoliumyl-substituted oligophosphanes. Building on this platform, we now report the synthesis of cationic diphosphanes and iso-tetraphosphanes *via* controlled coupling of $L_CP(R)Cl^+$ precursors. Using these chlorophosphanes as a starting point, we highlight in this contribution the generation of the symmetric diphosphanes ($(L_CPR)_2[OTf]_2$, Fig. 1-IV) and iso-tetraphosphanes ($(L_CPR)_3P[OTf]_3$, Fig. 1-V). Notably, this is the first report of a successful synthesis of branched oligophosphanes featuring cationic substituents. These substituents substantially alter the preferred reaction pathways of these phosphanes and electronically predispose selected P–P bonds toward fragmentation, leading to distinct products upon reaction with transition metal compounds or nucleophiles. In contrast to literature reports on di- and iso-tetraphosphanes, the synthesized compounds do not exhibit classical coordination to transition metals *via* the free electron pairs on the phosphorus atoms (*cf.* Fig. 1-I and III), but rather engage in selective P–P bond cleavage reactions.

Results and discussion

Syntheses and characterizations of imidazoliumyl-substituted chlorophosphanes, diphosphanes, and iso-tetraphosphanes

Our established protocol of using L_C-$SiMe_3$[OTf] **1**[OTf] as an "onio-transfer" reagent provides access to chlorophosphane salts **2a–c**[OTf] containing cationic imidazoliumyl substituents.[17,18] Accordingly, treatment of **1**[OTf] with a slight excess of the dichlorophosphate **3a–c** affords **2a–c**[OTf] in excellent to quantitative yield (Scheme 1).

The $^{31}P\{^1H\}$ NMR spectra of **2a–c**[OTf] each show a single, broad resonance (**2a**[OTf]: $\delta(P) = 55.6$ ppm; **2b**[OTf]: $\delta(P) = 48.8$ ppm; **2c**[OTf]: $\delta(P) = 24.0$ ppm), which are significantly upfield-shifted compared to **3a–c**. The resonance of **2c**[OTf] is downfield-shifted compared to **2b**[OTf] due to the mesomeric effect of the pyridyl substituent. Upon cooling to 250 K, the resonances of **2a–c**[OTf] each resolve into two singlet resonances. This is attributed to the presence of two rotamers, which originate from hindered rotation of the iPr-groups at the imidazoliumyl substituent. This assumption is supported by the observation of a splitting of the resonances of the iPr-groups in

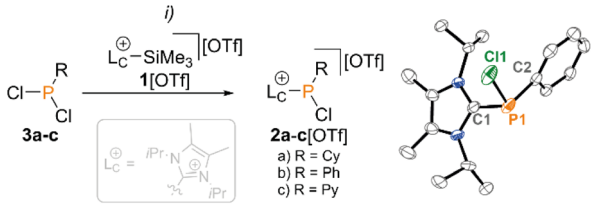

Scheme 1 Synthesis of imidazoliumyl-substituted chlorophosphanes **2a–c**[OTf] and the molecular structure of **2b**[OTf]·C_6H_5F (hydrogen atoms, solvate molecule, and anion are omitted for clarity, and ellipsoids are displayed at 50% probability). Selected bond lengths [Å] and angles [°]: C1–P1 1.827(3), P1–C2 1.822(2), P1–Cl1 2.0638(8), C1–P1–C2 100.78(9), C1–P1–Cl1 98.86(7), C2–P1 Cl1 102.83(7). (i) **2a**[OTf] (R = Cy): C_6H_5F, 70 °C, 3 d, 74%; **2b**[OTf] (R = Ph): C_6H_5F, 90 °C, 16 h, 74%; **2c**[OTf] (R = Py): C_6H_5F, 70 °C, 3 h, 99% (ref. 18).

the ^{1}H-NMR spectra at low temperatures and by a disordered iPr-group in the molecular structure of **2b**[OTf] (see SI, Section 2.1.2).

To better understand this behaviour, a conformer search for $\mathbf{2b}^+$ was conducted using the Conformer-Rotamer Ensemble Sampling Tool (CREST; see Fig. 2).[19] After geometry optimization (BP86-D4/def2-TZVP), two isoenergetic isomers were identified. The calculated rotational barrier in CH_2Cl_2 was 10.4 kcal mol^{-1}, which agrees well with the NMR-derived barrier (12.3 kcal mol^{-1}) at the coalescence temperature. The calculated chemical shift difference $\Delta\delta(P)$ is 3.0 ppm, which is also consistent with the experimental data ($\Delta\delta(P_{exp}) = 3.1$ ppm).

Both computationally disclosed conformers were also observed in the molecular structure of $\mathbf{2b}^+$ in the form of a disordered isopropyl group (see Scheme 1 and Fig. S6). As expected, the molecular structures (**2a,c**[OTf]: see SI) show the pyramidal bonding environment at the phosphorus atom, with typical P–Cl bond lengths ranging from 2.064(8) Å to 2.0770(13) Å, and P–C bonds which are comparable to those in known imidazoliumyl-substituted phosphanes.[17]

With larger quantities of **2a–c**[OTf] in hand, we explored the reduction reactions using 1,4-bis(trimethylsilyl)-1,4-dihydropyrazine (**4**), a reagent previously shown to be

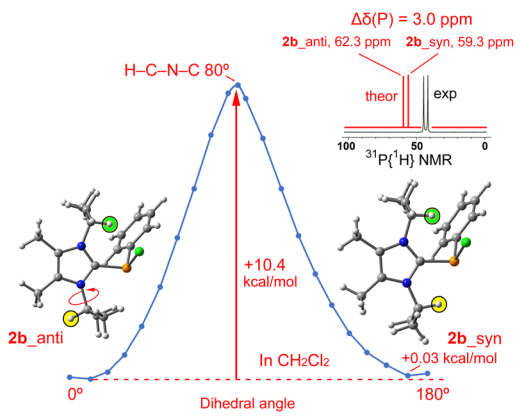

Fig. 2 Energy profile of the rotation of the lower iso-propyl substituent along the C–N bond in **2b**[OTf], with a comparison between calculated and experimental $^{31}P\{^1H\}$-NMR spectra of **2b**[OTf] in CD_2Cl_2 (top right insert).

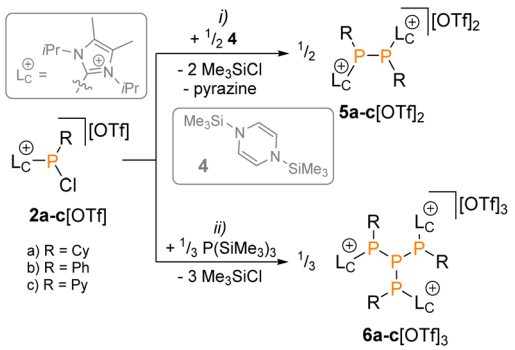

Scheme 2 Synthesis of diphosphane salts **5a–c**$[OTf]_2$ and iso-tetraphosphane salts **6a–c**$[OTf]_3$; (i) **5a**$[OTf]_2$: C_6H_5F, rt, 16 h, 63%; **5b**$[OTf]_2$: C_6H_5F, rt, 4 d, 78%; **5c**$[OTf]_2$: C_6H_5F, rt, 4 d, 87%; (ii) **6a**$[OTf]_3$: C_6H_5F, rt, 3 d, 76%; **6b**$[OTf]_3$: C_6H_5F, rt, 16 h, 81%; **6c**$[OTf]_3$: C_6H_5F, rt, 20 h, not isolated.

effective for reductive P–P bond formation.[14,20] The 2:1 reaction of **2a–c**[OTf] in C_6H_5F produced colourless or yellow precipitates over 16 h. After filtration and subsequent drying under vacuum, diphosphane salts **5a–c**$[OTf]_2$ were isolated in good yields (**5a**$[OTf]_2$: 63%; **5b**$[OTf]_2$: 78%; **5c**$[OTf]_2$: 87%; Scheme 2).

At ambient temperature, the $^{31}P\{^1H\}$-NMR spectra show a single broad resonance in each case (**5a**$[OTf]_2$: $\delta(P) = -50.0$ to -38.4 ppm; **5b**[OTf]: $\delta(P) = -47.9$ ppm; **5c**[OTf]: $\delta(P) = -43.0$ ppm). The signals are upfield-shifted compared to related neutral diphosphanes (*e.g.* Cy_2P–PCy_2: $\delta(P) = -21.0$ ppm; Ph_2P–PPh_2: $\delta(P) = -14.6$ ppm).[21] Upon cooling to 250 K, the broad resonances resolve into singlet resonances (**5b**$[OTf]_2$: $\delta(P) = -57.1$ ppm, $\delta(P) = -50.5$ ppm, $\delta(P) = -41.0$ ppm) and an AB spin system (**5b**$[OTf]_2$: $\delta(P_A) = -46.4$ ppm $\delta(P_B) = -43.3$ ppm, $^1J(PP) = -146$ Hz; Fig. 3e). This is attributed to the presence of three conformers, arising from hindered rotation around the N–C bond of the iPr groups.

A conformational analysis using CREST was performed on compound $\mathbf{5b}^{2+}$. The analysis identified three isomers with comparable energies. Fig. 3a–c presents the optimized geometries and relative energies, alongside the predicted $^{31}P\{^1H\}$-NMR spectra for these isomers. Two of the isomers are centrosymmetric, leading to an anticipated singlet resonance in the $^{31}P\{^1H\}$-NMR spectrum (labelled as $\mathbf{5b}^{2+}$(**b**) and $\mathbf{5b}^{2+}$(**c**); in Fig. 3b and c). The third isomer, denoted as $\mathbf{5b}^{2+}$(**a**), lacks symmetry and is expected to display an AB spin system in $^{31}P\{^1H\}$-NMR (Fig. 3d and e). These three isomers arise from rotation of the iPr groups marked in yellow in Fig. 3a–c. In contrast, the rotation of the green-marked groups leads to significantly higher-energy rotamers, resulting in diminished population. The predicted $^{31}P\{^1H\}$-NMR spectrum for this isomer mixture is shown in Fig. 3d. The calculated spectrum aligns with the experimental spectra. The close match of the expected coupling constant for $\mathbf{5b}^{2+}$(**a**; -144 Hz) and the experimental value (-146 Hz) strongly supports the presence of this non-symmetric rotamer in solution. The molecular structure of **5c**$[OTf]_2$ evidenced disordered isopropyl groups, confirming the presence of the computationally predicted conformers (see Fig. S24). The crystal structures of **5a–c**$[OTf]_2$ show an *anti*-conformation along the P–P bond (**5b**$[OTf]_2$: Fig. 4; **5a,c**$[OTf]_2$: see SI, Sections 2.2.1 and 2.2.3). The P–P bond lengths range from 2.2315(17) Å to 2.2581(7) Å, in line with P–P single bonds in neutral diphosphanes (Cy_2P–PCy_2 2.21 Å; Ph_2P–PPh_2 2.22 Å).[21,22]

Aiming at the construction of larger oligophosphorus scaffolds, we treated the chlorophosphanes **2a–c**[OTf] with an excess of $P(SiMe_3)_3$ in C_6H_5F. The reaction leads to the formation of colourless precipitates over the course of 1 to 3 days, which, after filtration, could be identified as the desired tricationic iso-tetraphosphane salts **6a,b**$[OTf]_3$ (see Scheme 2). **6a,b**$[OTf]_3$ were isolated in 76% and 81%, respectively. In contrast, the pyridyl-substituted derivative **6c**$[OTf]_3$ was found to decompose in solution, preventing its isolation. **6a,b**$[OTf]_3$

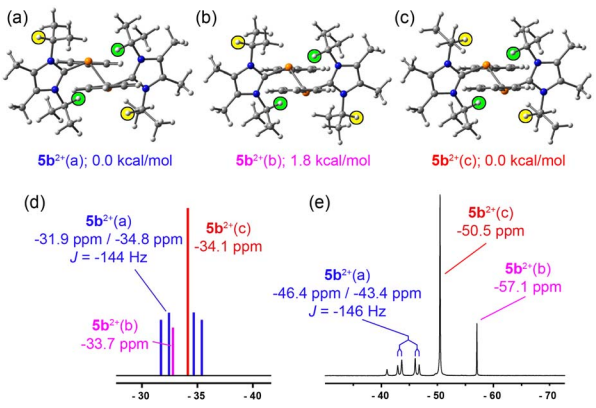

Fig. 3 (a–c) Conformers of $\mathbf{5b}^{2+}$ through rotation of the N–C bond of the iPr-groups obtained from conformer search and geometry optimization; (d) computationally obtained ^{31}P-NMR spectrum of the isomer mixture of $\mathbf{5b}^{2+}$; (e) $^{31}P\{^1H\}$-NMR spectrum of **5b**$[OTf]_2$ in CD_2Cl_2 at 250 K.

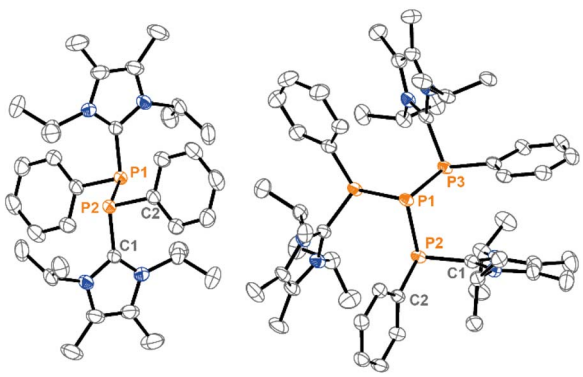

Fig. 4 Molecular structure cations $\mathbf{5b}^{2+}$ in **5b**$[OTf]_2$ (left) and $\mathbf{6b}^{3+}$ in **6b**$[OTf]_3$ $4CH_2Cl_2$ (right; one of two independent molecules of the asymmetric unit shown). Hydrogen atoms, solvate molecules, and anions are omitted for clarity; ellipsoids are set at 50% probability. Selected bond lengths [Å] and angles [°]: $\mathbf{5b}^{2+}$: P1–C1 1.8256(15), P1–P1 2.2581(7), P1–C2 1.8312(15), C1–P1–P1 98.57(5); $\mathbf{6b}^{3+}$: P2–C1 1.835(3), P1–P2 2.255(8), P2–C2 1.825(2), P1–P2–C1 101.91(8), P1–P2–C2 107.62(8), P2–P1–P3 89.35(3).

show AX_3-type spin systems in the $^{31}P\{^1H\}$-NMR spectra (AX_3 spin system: **6a**[OTf]$_3$ $\delta(P_A) = -87.4$ ppm, $\delta(P_X) = -57.7$ ppm, $^1J(PP) = -271$ Hz; **6b**[OTf]$_3$ $\delta(P_A) = -47.9$ ppm, $\delta(P_X) = -41.8$ ppm, $^1J(PP) = -130$ Hz). **6a**$^{3+}$ additionally shows dynamic behaviour at ambient temperature. The observed additional broad resonances resolve into an AX_3 pattern at 240 K ($\delta(P_A) = -84.0$ ppm, $\delta(P_X) = -41.5$ ppm, $^1J(PP) = -296$ Hz), which is attributed to a similar rotational behaviour of its isopropyl groups, as described above for **2a–c**[OTf]. Additional resonances at *ca.* −23 ppm are assigned to an unknown isomer formed by an exchange process, which could be monitored *via* ^{31}P–^{31}P EXSY NMR spectroscopy (see SI, Section 2.3.4). The resonances of **6b**[OTf]$_3$ exhibit second-order effects, as documented for related systems.[7,11] Compared to the neutral iso-tetraphosphane $(Cy_2P)_3P$ (AX_3: $\delta(P_A) = -108.9$ ppm, $\delta(P_X) = -5.2$ ppm; $^1J(PP) = -361.9$ Hz), the cationic analogues **6a,b**[OTf]$_3$ exhibit upfield shifted P_X resonances. Additionally, significantly smaller $|^1J(PP)|$ values are observed for the phenyl-substituted species **6b**$^{3+}$ compared to the cyclohexyl-substituted derivative **6a**$^{3+}$. This is attributed to the smaller steric volume of the phenyl substituent. Less steric congestion results in a diminished spatial overlap of the lone pairs on the outer phosphorus atoms, thereby reducing the electronic coupling between the central and terminal phosphorus atoms in **6b**$^{3+}$.[23]

Suitable crystals for X-ray diffraction analysis could be obtained by diffusion of Et_2O into a saturated CH_3CN (**6a**[OTf]$_3$) or CH_2Cl_2 (**6b**[OTf]$_3$) solution at −30 °C. The crystal structure of **6b**[OTf]$_3$ (Fig. 4) confirms the expected pyramidal coordination geometry at the central phosphorus atom. Due to the presence of two different substituents at the terminal phosphorus atoms, the cations **6a**$^{3+}$ and **6b**$^{3+}$ are chiral. The *rac*-diastereomer is observed in the single-crystal X-ray structure, with both enantiomers present in the unit cell. The P–P bond lengths (2.2315(17) Å to 2.2596(7) Å) are slightly elongated compared to neutral iso-tetraphosphanes.[10,11] In **6a**$^{3+}$, the imidazoliumyl-substituent and the lone pair of electron pair at the central phosphorus atom adopt an eclipsed arrangement. In contrast, cation **6b**$^{3+}$ exhibits a staggered conformation along the same axis, wherein the lone pairs on P1 and P2 are arranged in an antiperiplanar fashion.

Reactivity of imidazoliumyl-substituted diphosphanes 5a,b[OTf]$_2$ towards Pd(PPh$_3$)$_4$

The presence of two lone pairs in the dicationic diphosphanes **5a–c**[OTf]$_2$ motivated us to explore the coordination chemistry of these compounds towards selected transition metal complexes. Addition of a solution of Pd(PPh$_3$)$_4$ to **5b**[OTf]$_2$ in CH_2Cl_2 resulted in an immediate colour change to deep purple. Precipitation and washing of the obtained solid led to the isolation of the Pd-complex **7b**[OTf]$_2$ in 63% yield as a deep purple solid (see Scheme 3). For the analogous reaction of **5a**[OTf]$_2$, elevated temperatures of 120 °C and a prolonged reaction time were required. We attribute this to the increased steric bulk of the cyclohexyl substituents, which likely hampers Pd insertion into the P–P bond of **5a**$^{2+}$. Using this procedure, **7a**[OTf]$_2$ was isolated in 30% yield. It seems likely

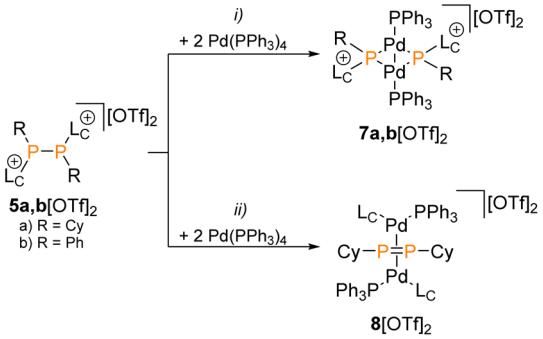

Scheme 3 Synthesis of complexes **7a,b**[OTf]$_2$ and diphosphene complex **8**[OTf]$_2$ (a: R = Cy; b: R = Ph); (i) **7a**[OTf]$_2$: toluene, 120 °C, 2 d, 30%; **7b**[OTf]$_2$: CH_2Cl_2, rt, 16 h, 63%; (ii) **8**[OTf]$_2$: $C_6H_4F_2$, 40 °C, 14d, 54%.

that **7a,b**[OTf]$_2$ are formed an oxidative insertion of two Pd atoms into the P–P bond of the diphosphane with concomitant release of six equivalents of PPh_3.

The Pd atoms in **7a,b**[OTf]$_2$ are in the formal oxidation state +I. The structural data indicate a Pd–Pd interaction (**7b**$^{2+}$: Pd–Pd 2.584(19) Å). In the $^{31}P\{^1H\}$-NMR spectra, the complexes show two sets of A_2X_2 spin systems (**7b**[OTf]$_2$: $\delta(P_A) = 24.5$ ppm, $\delta(P_X) = 105.33$ ppm, $^2J(AX) = 44$ Hz; $\delta(P_A) = 25.9$ ppm, $\delta(P_X) = 111.5$ ppm, $^2J(AX) = 41$ Hz; for **7a**[OTf]$_2$, see SI Section 2.4), attributed to the *rac* and *meso* stereoisomers resulting from the different orientation of the imidazoliumyl-substituents. The P_A resonances show the typical chemical shift of PPh_3 ligands at palladium. The P_X resonances of the bridging phosphanide moieties show a substantial downfield shift compared to chemical shifts of related imidazoliumyl-substituted phosphanides,[15] including bridging phosphanides in three-membered metallacycles.[24] In the case of **7b**[OTf]$_2$, the isomer with the more downfield-shifted P_X resonances is the major isomer (84/16), whereas **7a**[OTf]$_2$ shows an inverted ratio (10/90). Interestingly, in both cases, no interconversion between isomers was observed, even at elevated temperatures or in highly polar solvents. Although these conditions typically promote isomerization in phosphorus–metal complexes, this does not seem to occur with **7a**[OTf]$_2$.[25]

Suitable crystals for X-ray diffraction analysis could be obtained by diffusion of *n*-pentane into a saturated CH_2Cl_2 solution at −30 °C. The molecular structure of the *meso* isomer of **7b**[OTf]$_2$ is depicted in Fig. 5. In the bicyclic P_2Pd_2 core, the two imidazoliumyl-substituted phosphanide units bridge the palladium atoms, which are connected through a short Pd–Pd contact (2.584(19) Å), indicating metal–metal interaction as known from related compounds.[26] Additionally, one remaining PPh_3 ligand is coordinated each of the Pd-atoms.

Although the Pd–Pd bond length is comparably short,[27] the calculated Wiberg Bond Index (WBI) is fairly low (0.24), indicating only a weak interaction of the two palladium atoms (see SI Section 3.2).

During our attempts to isolate pure **7b**[OTf]$_2$, we observed the formation of a side-product at elevated temperatures. ^{31}P-

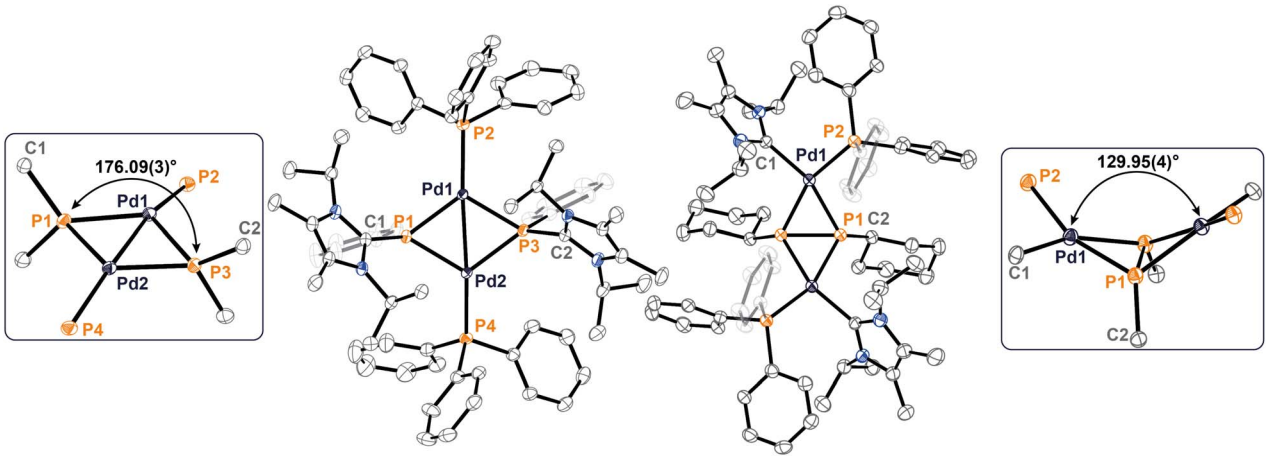

Fig. 5 Molecular structures of cations $\mathbf{7b}^{2+}$ in $\mathbf{7b}[OTf]_2 \cdot 4CH_2Cl_2$ (left) and $\mathbf{8}^{2+}$ in $\mathbf{8}[OTf]_2 \cdot 2C_6H_4F_2 \cdot Et_2O$ (right); insets show detailed coordination environment. Hydrogen atoms, solvate molecules, and anions are omitted for clarity. Ellipsoids are set at 50% probability. Selected bond lengths [Å]and angles [°]: $\mathbf{7b2}^{2+}$: Pd–Pd 2.584(19), P1–C1 1.840(3), P3–C3 1.834(3), P2–Pd1 2.3011(6), P4–Pd2 2.2988(6), Pd1–P1–Pd2 67.78(18), Pd1–P3–Pd2 67.80(18); $\mathbf{82}^{2+}$: P1–P1 2.1160(12), P2–Pd 2.3213(6), C1–Pd 2.061(2), Pd–Pd 3.8007(8), P1–Pd–P1 53.54(4), P–Pd–P plane fold angle 129.95(4).

NMR investigations of the reaction mixture of $\mathbf{5a}[OTf]_2$ with $Pd(PPh_3)_4$ stirred at 80 °C indicate the formation of dinuclear $\mu_2(\eta^2{:}\eta^2)$-diphosphene complex $\mathbf{8}[OTf]_2$.

The complex is a structural isomer of $\mathbf{7b}[OTf]_2$ and is formed by oxidative addition of the P–C bond of the imidazoliumyl substituent to Pd, rather than the P–P bond. Such P–C activation is rare and typically occurs only as a side reaction with phosphane ligands in organometallic chemistry.[28]

A selective synthesis of $\mathbf{8}[OTf]_2$ was achieved by stirring the reaction mixture of $\mathbf{5a}[OTf]_2$ with two equivalents of $Pd(PPh_3)_4$ at 40 °C for 14 days in *ortho*-$C_6H_4F_2$. The ^{31}P-NMR spectrum $\mathbf{8}[OTf]_2$ shows broad resonances at $\delta(P_A) = -11.7$ ppm and $\delta(P_X) = 18.2$ ppm, which resolve at higher temperatures to an AA'XX' spin system (fitted iteratively; see SI, Section 2.4.3). The resonance of the diphosphene moiety (P_A) is shifted downfield compared to the related molybdenum complex $[(Cp)_2Mo_2(CO)_4(PPh_2)_2]$ ($\delta(P) = -94$ ppm)[29,30] and the large $^1J(PP)$ coupling constant of −489 Hz is typical for diphosphene complexes.[31] In the ^{31}P-NMR spectrum, a minor isomer is observed, which is presumed to be the corresponding *meso* isomer.

Single crystals of $\mathbf{8}[OTf]_2$ suitable for X-ray analysis were obtained by slow diffusion of Et_2O into a saturated *ortho*-$C_6H_4F_2$ solution at −30 °C (see Fig. 5). The molecular structure revealed the *rac* isomer, with a central *cis*-substituted diphosphene coordinated to two palladium atoms in η^2 mode. The palladium atoms are additionally coordinated by one L_C ligand and one PPh_3 ligand. The P–P bond length of 2.1160(12) Å is in the expected range for diphosphene complexes.[31] The central four-membered Pd_2P_2 ring is puckered, adopting a "butterfly" conformation (fold angle between the P–Pd–P planes = 129.95(4)°; Fig. 5). The Pd–C bond (2.061(2) Å) aligns well with those in known N-heterocyclic carbene palladium complexes.[32] Only a few related complexes have been reported, which feature a similar diphosphene ligand bridging two transition-metal atoms, such as Fe, Mo and Ta.[29,30,33,34] The Pd–Pd distance of 3.8007(8) Å is significantly larger than the sum of the van der Waals radii (3.26 Å),[35] indicating that there is no significant Pd···Pd interaction in $\mathbf{8}^{2+}$.

It is noteworthy that the formation of $\mathbf{8}[OTf]_2$ from $\mathbf{5b}[OTf]_2$ is highly selective. The mechanism likely involves a nucleophilic attack by a Pd atom on $\mathbf{5b}^{2+}$, which ultimately results in the cleavage of two P–P bonds. The DFT-calculated frontier molecular orbitals of $\mathbf{5b}^{2+}$ (RI-BP86-D4/def2-TZVP level, Fig. 6) show that the P–P bonds exhibit strong antibonding behaviour in the LUMO, indicating pronounced electrophilic character. The detailed mechanism presently remains unknown. However, it is noteworthy that $\mathbf{8}[OTf]_2$ could not be generated from the isomeric complex $\mathbf{7b}[OTf]_2$, which remained stable in solution at elevated temperatures for days. This indicates that $\mathbf{8}[OTf]_2$ does not form *via* isomerization from $\mathbf{7b}[OTf]_2$.

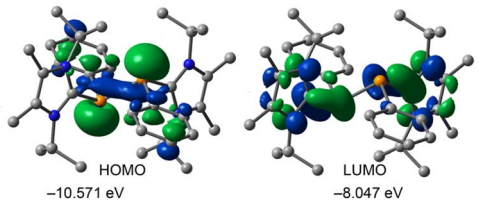

Fig. 6 Frontier molecular orbitals of $\mathbf{5b}^{2+}$, resembling the high antibonding character of the LUMO.

Reactivity of imidazoliumyl-substituted iso-tetraphosphane $\mathbf{6a}[OTf]_3$ towards metal chlorides and nucleophiles

We were also keen to investigate the potential follow-up chemistry of the iso-tetraphosphanes $\mathbf{6a}[OTf]_3$. Consistent with the observations for $\mathbf{5b}^{2+}$, the frontier molecular orbital analysis of $\mathbf{6a}^{3+}$ indicated a rather electrophilic character of the iso-tetraphosphane framework (Fig. 7). The LUMO is notably

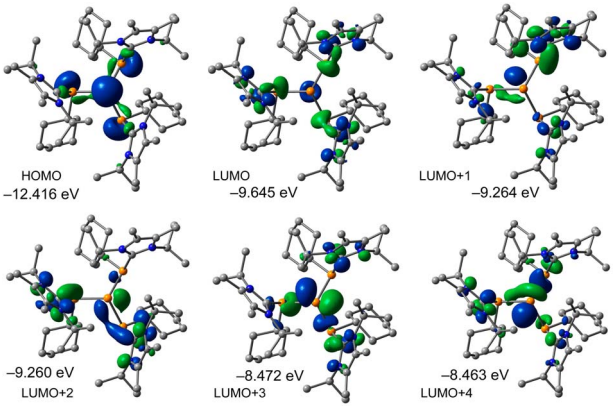

Fig. 7 Frontier molecular orbitals of $\mathbf{6a}^{3+}$, resembling the high anti-bonding character of the LUMO and LUMO+1/+2.

delocalized, featuring contributions that exhibit antibonding character of the P–P bonds. Across the HOMO through LUMO+4, there is a significant involvement of the iso-tetraphosphane core. To probe this predicted electrophilicity experimentally, we studied the reactivity of **6a**$[OTf]_3$ with nucleophiles. Reactions of **6a**$[OTf]_3$ with $Pd(PPh_3)_4$ showed no conversion, even at 60 °C. In contrast, $Pd_2Cl_2(allyl)_2$ triggered reactivity (see Scheme 4). The initially colourless reaction mixture of **6a**$[OTf]_3$ with 0.5 equivalents of $Pd_2Cl_2(allyl)_2$ turned orange within 5 min. The ^{31}P-NMR spectrum of the reaction mixture revealed two new A_2B spin systems ($\delta(P_A) = -61.3$ ppm, $\delta(P_B) = -16.1$ ppm, $^1J(PP) = -323$ Hz; and $\delta(P_A) = -57.6$ ppm, $\delta(P_B) = -25.1$ ppm, $^1J(PP) = -321$ Hz), displaying higher-order coupling effects.[7,11,36] Additionally, a broad singlet resonance at $\delta(P) = 55.6$ ppm appeared, which was assigned to the chlorophosphane $\mathbf{2a}^+$. This observation indicates that the palladium complex is formed *via* a chloride-induced P–P bond cleavage reaction of **6a**$[OTf]_3$.

Following solvent removal and toluene extraction of **2a**[OTf], complex **9**$[OTf]_2$ was obtained as a pure orange solid in 59% yield. The two A_2X spin systems are observed in the ^{31}P-NMR spectrum of the isolated compound in a 44 : 56 ratio. These correspond to the *rac* and *meso* diastereomers, which originate from different configurations of the P atoms in the triphosphanide ligand present in **9**$[OTf]_2$.[37]

The susceptibility of iso-tetraphosphane **6a**$[OTf]_3$ towards chloride-induced P–P cleavage motivated further reactions with transition metal chlorides. To this end, we treated **6a**$[OTf]_3$ with $AuCl(PPh_3)$, assuming that a similar fragmentation process might occur (Scheme 4). As expected, the reaction of **6a**$[OTf]_3$ with $AuCl \cdot PPh_3$ (1 equiv.) leads to the formation of **2a**[OTf] and gold complex **10**$[OTf]_2$. **10**$[OTf]_2$ was isolated as an analytically pure, colourless powder (88% yield) after removal of all volatiles and repeated washing with toluene.

At room temperature, the ^{31}P NMR spectrum of **10**$[OTf]_2$ shows broad signals. Upon cooling to 190 K, four distinct spin systems are resolved, corresponding to four isomers: *rac*, *meso,* and the rotamers *rac*′ and *meso*′ (see SI, Fig. S69). Both *rac* isomers exhibit AMNX spin systems with comparable features, while the symmetric *meso* isomer displays an AM_2X spin system. The *meso* isomer also exhibits an AM_2X spin system, with only slight differences in chemical shift between the P_M and P_N atoms ($\delta(P_M) = -21.6$ ppm, $\delta(P_N) = -21.3$ ppm). The central phosphorus atom shows a downfield-shifted resonance ($\delta(P_A) = -78.9$ to -84.5 ppm) compared to the anionic ligand $[P(tBu_2P)_2]^-$ ($\delta(P_A) = -134$ ppm),[8] suggesting its coordination to the metal center. This assignment is corroborated by the crystal structure of **10**$[OTf]_2$ (see Fig. 8), which shows the *rac* isomer with gold coordinated linearly by the PPh_3 ligand and the central P atom of the triphosphanide ligand (P2–Au–P4 angle of 172.38(5)°). The P–P bond lengths (2.210(2) Å and 2.207(2) Å) fall within the range expected for P–P single bonds.[38] A slight elongation of the P–P bond is attributed to reduced negative hyperconjugation from the central phosphorus atom due to the lower electron density upon metal coordination.

Based on the successful synthesis of triphosphanide complexes **9**$[OTf]_2$ and **10**$[OTf]_2$, we explored the isolation of the free ligand. At

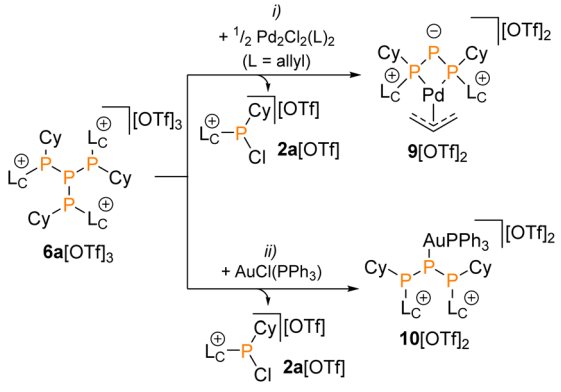

Scheme 4 Synthesis of palladium complex **9**$[OTf]_2$ and gold complex **10**$[OTf]_2$ from **6a**$[OTf]_3$ *via* chloride-induced P–P bond cleavage; (i) – **2a**[OTf], CH_3CN, rt, 30 min, 59%; (ii) – **2a**[OTf], CH_3CN, −30 °C, 30 min, 88%.

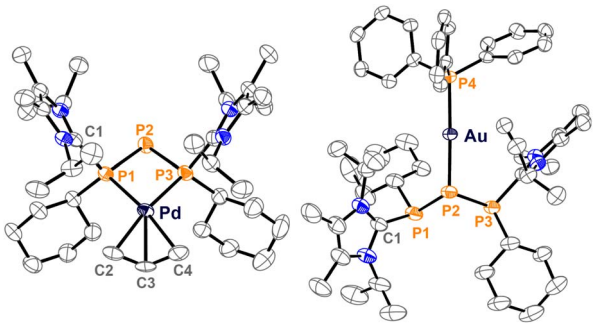

Fig. 8 Molecular structures of **9**$[OTf]_2 \cdot C_6H_5F \cdot 0.5THF$ and **10**$[OTf]_2 \cdot 1.5CH_2Cl_2 \cdot 2MeCN$. Hydrogen atoms, solvate molecules, and anions are omitted for clarity. Ellipsoids are set at 50% probability. Selected bond lengths [Å] and angles [°]: $\mathbf{9}^{2+}$: P1–P2 2.1527(13), P2–P3 2.1544(13), C1–P1 1.857(4), C2–Pd 2.189(4), C3a–Pd 2.169(6), C3b–Pd 2.169(12), C4–Pd 2.182(5), P1–P2–P3 85.40(5), P1–Pd–P3 74.47(3); $\mathbf{10}^{2+}$ P1–P2 2.210(2), P2–P3 2.207(2), C1–P1 1.845(6), Au–P2 2.3302(12), P4–Au 2.3028(12), P1–P2–P3 91.21(8), P2–Au–P4 172.38(5).

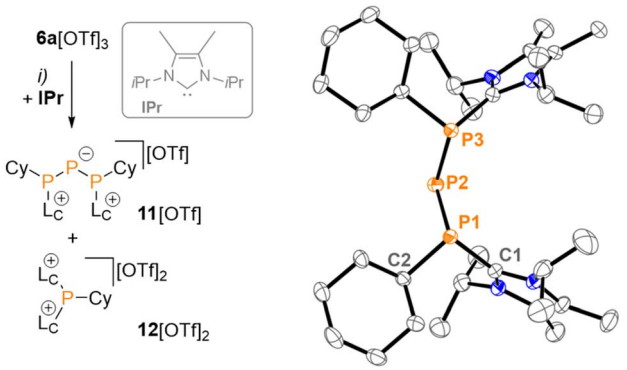

Fig. 9 Synthesis of triphosphanide **11**[OTf] (left) and molecular structure of $\mathbf{11}^{+}$ in **11**[OTf]·CH_2Cl_2 (right); (i) $C_6H_4F_2$, 60 min, 65%. Hydrogen atoms, solvate molecules, and anions are omitted for clarity. Ellipsoids are set at 50% probability. Selected bond lengths [Å] and angles [°]: P1–P2 2.1592(7), P2–P3 2.1606(7), C1–P1 1.8561(18), C2–P1 1.8738(18), P1–P2–P3 93.65(7).

first, we tested the reaction of **6a**[OTf]$_3$ with Ph_4P[Cl] as a soluble chloride source. However, the reaction proved unselective, forming several products (see the SI, Section 2.5.5). Using the N-heterocyclic carbene IPr instead of chloride resulted in the clean formation of the desired triphosphanide salt **11**[OTf] and bis(imidazoliumyl) phosphane salt **12**[OTf]$_2$ (Fig. 9). **12**[OTf]$_2$ is formed by nucleophilic attack of IPr on a L_CPCy unit of $\mathbf{6a}^{3+}$. The formation of **12**[OTf]$_2$ was confirmed by ^{31}P-NMR spectroscopy, which showed an identical resonance $\delta(P) = -38.2$ ppm as a sample independently synthesized *via* an alternative route (see SI, Section 2.5.4).[39] Triphosphanide salt **11**[OTf] was isolated as a yellow crystalline solid 65% yield after recrystallization from THF. The ^{31}P-NMR spectrum of **11**[OTf] at room temperature shows two broad AX_2 spin systems, consistent with a *rac*, *meso* mixture (*meso*: $\delta(P_A) = -135.2$ ppm, $\delta(P_X) = -3.2$ ppm, $^1J(PP) = -316$ Hz; *rac*: $\delta(P_A) = -130.6$ ppm, $\delta(P_X) = -6.9$ ppm, $^1J(PP) = -315$ Hz). Upon cooling to 190 K, four spin systems emerge, corresponding to the *rac* and *meso* diastereomers as well as their inverted rotamers *rac*′ and *meso*′, analogous to the behaviour for **10**[OTf]$_2$.

Crystals of **11**[OTf] suitable for X-ray diffraction analysis were obtained by slow diffusion of *n*-pentane into a saturated solution in CH_2Cl_2/C_6H_5F (v/v = 1 : 1) at −30 °C. The molecular structure is depicted in Fig. 9, confirming the presence of the *meso* diastereomer. The structure features the two nearly identical P–P bonds (2.1591(6) Å and 2.1606(6) Å) and a central P1–P2–P3 angle of 93.65(7)°, consistent with a flexible, uncoordinated triphosphanide framework.[40]

Conclusions

The present work demonstrates that onio substitution not only stabilizes cationic oligophosphorus frameworks, but can also electronically predispose specific P–P bonds toward selective fragmentation pathways. Using the chlorophosphane salts **2a–c**[OTf], we have isolated the dicationic diphosphane salts **5a–c**[OTf]$_2$ and the first cationic iso-tetraphosphane salts **6a,b**[OTf]$_3$. Reactivity studies of **5a,b**[OTf]$_2$ towards $Pd(PPh_3)_4$ showed competing oxidative additions of either a P–P bond or a P–C bond, yielding **7a,b**[OTf]$_2$ or the unusual $\mu_2(\eta^2{:}\eta^2)$-diphosphene complex **8a**[OTf]$_2$. The significant disparity in reactivity between **5a**[OTf]$_2$ and **5b**[OTf]$_2$ raises questions regarding the general stability of imidazoliumyl-substituted phosphanes in transition metal complexes, particularly in catalytic applications.

The use of transition metal chlorides in reactions with the readily accessible **6a**[OTf]$_3$ enabled the selective generation of cationic triphosphanide complexes. Two distinct coordination motifs were identified: a four-membered metallacycle in the case of palladium (**9**[OTf]$_2$) and a linear coordination to the central phosphorus atom in the case of gold (**10**[OTf]$_2$), showcasing the versatility of the triphosphanide framework. Motivated by these findings, we developed a direct route to the free, non-coordinated triphosphanide ligand **11**[OTf], whose flexibility and structural integrity suggest a rich coordination chemistry yet to be explored.

Author contributions

J. F., K. S., R. W., and J. J. W. conceptualized the topic. J. F. and C. T. conducted the experiments and optimized the syntheses, isolations, and purifications. R. M. G. and A. F. were responsible for computational investigations. J. F., F. H. and J. J. W. were responsible for collecting X-ray data and refinement. K. S. and J. J. W. conceived, oversaw, and directed the project. J. F., K. S. and J. J. W. prepared the initial draft of the paper. A. F., R. W. and J. J. W. acquired funding. All authors discussed and analyzed the results and contributed to the editing of the manuscript.

Conflicts of interest

There are no conflicts to declare.

Data availability

The data supporting the findings of this study, including CIF files, NMR spectra, and computational details, are available in the supplementary information (SI). Additional data can be obtained from the corresponding author upon reasonable request. Supplementary information is available. See DOI: https://doi.org/10.1039/d6sc02577c.

CCDC 2524560–2524572 contain the supplementary crystallographic data for this paper.[41a–m]

Acknowledgements

This work was supported by the German Science Foundation (DFG grant numbers WE 4621/3-2 and WO1496/7-2). A. F. and R. M. G. thank the MICIU/AEI of Spain (project PID2023-148453NB-I00 FEDER funds) for financial support. J. F. and F. H. thank the Graduate Academy of TU Dresden for financial support. Philipp Lange is acknowledged for performing elemental analyses. TU Dresden is also thanked for its financial support.

Notes and references

1 (*a*) M. Alcarazo, *Chem.–Eur. J.*, 2014, **20**, 7868; (*b*) L. D. M. Nicholls and M. Alcarazo, *Chem. Lett.*, 2019, **48**, 1.

2 K. Schwedtmann, G. Zanoni and J. J. Weigand, *Chem. Asian J.*, 2018, **13**, 1388.

3 (*a*) W. Hieber and R. Kummer, *Z. Anorg. Allg. Chem.*, 1966, **344**, 292; (*b*) J. A. S. Howell, M. G. Palin, P. McArdle, D. Cunningham, Z. Goldschmidt, H. E. Gottlieb and D. Hezroni-Langerman, *Inorg. Chem.*, 1993, **32**, 3493; (*c*) R. Giannandrea, P. Mastrorilli, C. F. Nobile and M. Dilonardo, *Inorg. Chim. Acta*, 1996, **249**, 237; (*d*) S. J. Geier and D. W. Stephan, *Chem. Commun.*, 2010, **46**, 1026.

4 (*a*) L. J. Arnold, L. Main and B. K. Nicholson, *Appl. Organomet. Chem.*, 1990, **4**, 503; (*b*) O. Kühl, S. Blaurock and E. Hey-Hawkins, *Z. Anorg. Allg. Chem.*, 1999, **625**, 1517; (*c*) Y. Miyake, Y. Nomaguchi, M. Yuki and Y. Nishibayashi, *Organometallics*, 2007, **26**, 3611; (*d*) D. Tofan and C. C. Cummins, *Chem. Sci.*, 2012, **3**, 2474; (*e*) S. Molitor, C. Mahler and V. H. Gessner, *New J. Chem.*, 2016, **40**, 6467.

5 A. M. Caminade, J. P. Majoral and R. Mathieu, *Chem. Rev.*, 1991, **91**, 575.

6 (*a*) M. Scheer, S. Gremler, E. Herrmann and P. G. Jones, *J. Organomet. Chem.*, 1991, **414**, 337; (*b*) V. Balema, H. Goesmann, E. Matern and G. Fritz, *Z. Anorg. Allg. Chem.*, 1996, **622**, 35; (*c*) W. S. Sheldrick, *Acta Crystallogr., Sect. B*, 1976, **B32**, 308; (*d*) W. S. Sheldrick, S. Morton and O. Stelzer, *Z. Anorg. Allg. Chem.*, 1981, **475**, 232; (*e*) M. Baacke, S. Morton, G. Johannsen, N. Weferling and O. Stelzer, *Chem. Ber.*, 1980, **113**, 1328; (*f*) R. Schoemaker, K. Schwedtmann, A. Franconetti, A. Frontera, F. Hennersdorf and J. J. Weigand, *Chem. Sci.*, 2019, **10**, 11054.

7 G. Fritz, K. Stoll, W. Hönle and H. G. V. Schnering, *Z. Anorg. Allg. Chem.*, 1987, **544**, 127.

8 G. Fritz and T. Vaahs, *Z. Anorg. Allg. Chem.*, 1987, **553**, 85.

9 (*a*) A. H. Cowley, S. M. Dennis, S. Kamepalli, C. J. Carrano and M. R. Bond, *J. Organomet. Chem.*, 1997, **529**, 75; (*b*) M. Scheer, St. Gremler, E. Herrmann, U. Grünhagen, M. Dargatz and E. Kleinpeter, *Z. Anorg. Allg. Chem.*, 1991, **600**, 203; (*c*) M. Baudler, G. Reuschenbach and J. Hahn, *Z. Anorg. Allg. Chem.*, 1981, **482**, 27.

10 G. Fritz, E. Matern, H. Krautscheid, R. Ahlrichs, J. W. Olkowska and J. Pikies, *Z. Anorg. Allg. Chem.*, 1999, **625**, 1604.

11 K.-O. Feldmann, R. Fröhlich and J. J. Weigand, *Chem. Commun.*, 2012, **48**, 4296.

12 (*a*) C. A. Dyker and N. Burford, *Chem. Asian J.*, 2008, **3**, 28; (*b*) M. Donath, F. Hennersdorf and J. J. Weigand, *Chem. Soc. Rev.*, 2016, **45**, 1145.

13 C. Taube, K. Schwedtmann, M. Noikham, E. Somsook, F. Hennersdorf, R. Wolf and J. J. Weigand, *Angew. Chem. Int. Ed.*, 2020, **59**, 3585.

14 K. Schwedtmann, J. Haberstroh, S. Roediger, A. Bauzá, A. Frontera, F. Hennersdorf and J. J. Weigand, *Chem. Sci.*, 2019, **10**, 6868.

15 T. Krachko and J. C. Slootweg, *Eur. J. Inorg. Chem.*, 2018, **2018**, 2734.

16 (*a*) O. Back, B. Donnadieu, P. Parameswaran, G. Frenking and G. Bertrand, *Nat. Chem.*, 2010, **2**, 369; (*b*) A. Hermannsdorfer, D. W. Stephan and M. Driess, *Chem. Commun.*, 2018, **54**, 13523; (*c*) A. M. Tondreau, Z. Benkő, J. R. Harmer and H. Grützmacher, *Chem. Sci.*, 2014, **5**, 1545; (*d*) K. Schwedtmann, M. H. Holthausen, C. H. Sala, F. Hennersdorf, R. Fröhlich and J. J. Weigand, *Chem. Commun.*, 2016, **52**, 1409.

17 J. J. Weigand, K.-O. Feldmann and F. D. Henne, *J. Am. Chem. Soc.*, 2010, **132**, 16321.

18 J. Fidelius, K. Schwedtmann, S. Schellhammer, J. Haberstroh, S. Schulz, R. Huang, M. C. Klotzsche, A. Bauzá, A. Frontera, S. Reineke and J. J. Weigand, *Chem*, 2024, **10**, 644.

19 P. Pracht, F. Bohle and S. Grimme, *Phys. Chem. Chem. Phys.*, 2020, **22**, 7169.

20 L. P. Ho, A. Nasr, P. G. Jones, A. Altun, F. Neese, G. Bistoni and M. Tamm, *Chem.–Eur. J.*, 2018, **24**, 18922.

21 D. L. Dodds, M. F. Haddow, A. G. Orpen, P. G. Pringle and G. Woodward, *Organometallics*, 2006, **25**, 5937.

22 A. Dashti-Mommertz and B. Neumüller, *Z. Anorg. Allg. Chem.*, 1999, **625**, 954.

23 M. Baudler, G. Reuschenbach, D. Koch and B. Carlsohn, *Chem. Ber.*, 1980, **113**, 1264.

24 O. Kühl, *Phosphorus-31 NMR Spectroscopy*, Springer, Berlin, Heidelberg, 2009.

25 C. Taube, J. Fidelius, K. Schwedtmann, C. Ziegler, F. Kreuter, L. Loots, L. J. Barbour, R. Tonner-Zech, R. Wolf and J. J. Weigand, *Angew. Chem., Int. Ed.*, 2023, **62**, e202306706.

26 (*a*) A. M. Arif, D. E. Heaton, R. A. Jones and C. M. Nunn, *Inorg. Chem.*, 1987, **26**, 4228; (*b*) M. Sommovigo, M. Pasquali, P. Leoni and U. Englert, *Inorg. Chem.*, 1994, **33**, 2686.

27 N. W. J. Scott, M. J. Ford, C. Schotes, R. R. Parker, A. C. Whitwood and I. J. S. Fairlamb, *Chem. Sci.*, 2019, **10**, 7898.

28 Y. H. Lee and B. Morandi, *Coord. Chem. Rev.*, 2019, **386**, 96.

29 D. Fenske and K. Merzweiler, *Angew. Chem.*, 1986, **98**, 357.

30 D. Fenske and K. Merzweiler, *Angew. Chem., Int. Ed.*, 1986, **25**, 338.

31 L. Weber, *Chem. Rev.*, 1992, **92**, 1839.

32 M. S. Viciu, R. F. Germaneau, O. Navarro-Fernandez, E. D. Stevens and S. P. Nolan, *Organometallics*, 2002, **21**, 5470.

33 A. H. Cowley, D. M. Giolando, C. M. Nunn, M. Pakulski, D. Westmoreland and N. C. Norman, *Dalton Trans.*, 1988, 2127.

34 S. Blaurock and E. Hey-Hawkins, *Eur. J. Inorg. Chem.*, 2002, **2002**, 2975.

35 A. Bondi, *J. Phys. Chem.*, 1964, **68**, 441.

36 C. E. Averre, M. P. Coles, I. R. Crossley and I. J. Day, *Dalton Trans.*, 2012, **41**, 278.

37 (*a*) L.-M. Frenzel, C. Bruhn and R. Pietschnig, *Inorg. Chim. Acta*, 2021, **516**, 120091; (*b*) R. Franz, D. Gál, C. Bruhn, Z. Kelemen and R. Pietschnig, *Adv. Sci.*, 2024, **11**, e2306805.

38 A. F. Holleman, N. Wiberg and E. Wiberg, *Lehrbuch der Anorganischen Chemie*, Walter de Gruyter, 2007.
39 (*a*) C. L. B. Macdonald, J. F. Binder, A. Swidan, J. H. Nguyen, S. C. Kosnik and B. D. Ellis, *Inorg. Chem.*, 2016, **55**, 7152; (*b*) M. Azouri, J. Andrieu, M. Picquet and H. Cattey, *Inorg. Chem.*, 2009, **48**, 1236.
40 (*a*) G. Fritz, T. Vaahs, W. Hönle and H. G. v. Schnering, *Z. Anorg. Allg. Chem.*, 1987, **552**, 34; (*b*) G. Fritz, J. Härer and K. H. Scheider, *Z. Anorg. Allg. Chem.*, 1982, **487**, 44.
41 (*a*) CCDC 2524560: Experimental Crystal Structure Determination, 2026, DOI: 10.5517/ccdc.csd.cc2qr0fy; (*b*) CCDC 2524561: Experimental Crystal Structure Determination, 2026, DOI: 10.5517/ccdc.csd.cc2qr0gz; (*c*) CCDC 2524562: Experimental Crystal Structure Determination, 2026, DOI: 10.5517/ccdc.csd.cc2qr0h0; (*d*) CCDC 2524563: Experimental Crystal Structure Determination, 2026, DOI: 10.5517/ccdc.csd.cc2qr0j1; (*e*) CCDC 2524564: Experimental Crystal Structure Determination, 2026, DOI: 10.5517/ccdc.csd.cc2qr0k2; (*f*) CCDC 2524565: Experimental Crystal Structure Determination, 2026, DOI: 10.5517/ccdc.csd.cc2qr0l3; (*g*) CCDC 2524566: Experimental Crystal Structure Determination, 2026, DOI: 10.5517/ccdc.csd.cc2qr0m4; (*h*) CCDC 2524567: Experimental Crystal Structure Determination, 2026, DOI: 10.5517/ccdc.csd.cc2qr0n5; (*i*) CCDC 2524568: Experimental Crystal Structure Determination, 2026, DOI: 10.5517/ccdc.csd.cc2qr0p6; (*j*) CCDC 2524569: Experimental Crystal Structure Determination, 2026, DOI: 10.5517/ccdc.csd.cc2qr0q7; (*k*) CCDC 2524570: Experimental Crystal Structure Determination, 2026, DOI: 10.5517/ccdc.csd.cc2qr0r8; (*l*) CCDC 2524571: Experimental Crystal Structure Determination, 2026, DOI: 10.5517/ccdc.csd.cc2qr0s9; (*m*) CCDC 2524572: Experimental Crystal Structure Determination, 2026, DOI: 10.5517/ccdc.csd.cc2qr0tb.